Inorganic Chemistry

ARTICLE

pubs.acs.org/IC

# Charge Transfer and Intraligand Excited State Interactions in Platinum-Sensitized Dithienylethenes

Matthew N. Roberts,[†] Jeffrey K. Nagle,[‡] Marek B. Majewski,[†] Jeremy G. Finden,[§] Neil R. Branda,*[,§] and Michael O. Wolf*[,†]

[†]Department of Chemistry, University of British Columbia, Vancouver, British Columbia V6T 1Z1, Canada

[‡]Department of Chemistry, Bowdoin College, Brunswick, Maine 04011, United States

[§]Department of Chemistry, Simon Fraser University, Burnaby, British Columbia V5A 1S6, Canada

Supporting Information

**ABSTRACT:** The photophysical behavior for two photochromic Pt-terpyridine acetylide complexes containing pendant dithienylethenes (DTEs) bound to the metal through the alkynyl linkage is presented. Selective excitation of the Pt complex with visible light resulted in the metal-sensitized ring closing of the DTE unit. The central purpose of this study was to understand how excited state interactions govern the photophysics by correlating differences in the linkage of the two components with differences in the intramolecular energy transfer processes that occur between the Pt complex and the DTE. A series of model complexes without photochromic ligands were prepared and studied to elucidate the contributions of the triplet metal-to-ligand charge transfer and triplet intraligand states. It is demonstrated that reducing the orbital overlap of the metal-based and intraligand states by lengthening the linkage and eliminating a conjugated pathway is effective at dramatically decreasing the efficiency of intramolecular energy transfer. This is evidenced by the appearance of Pt-terpyridine based phosphorescence and a significant decrease in the observed rate of metal-sensitized ring closing of the DTE.

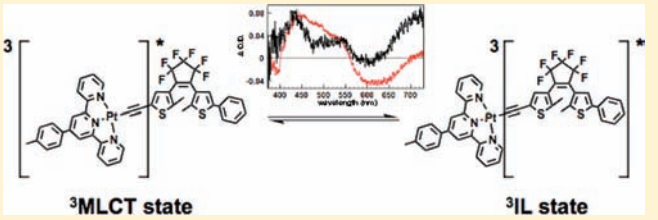


## INTRODUCTION

Photoresponsive materials that integrate photochromic organic compounds with metal coordination complexes are significant because the combination of the electronic and optical properties of each component gives rise to characteristics not found in either the organic or inorganic species alone.[1−3] The ground and excited state interactions between the components govern the overall electro-optical properties of the hybrid system; therefore, the choice of each building block is an essential consideration when designing this type of material. Successful modulation of a metal complex's properties by toggling the photoswitch between its two metastable states has been demonstrated,[4−9] while others have focused on the ability of a metal complex to affect the switching behavior of the photochromic unit.[10−14] In both cases, the identity of the metal and the linkage between the two components are primary factors in determining the types of interactions that exist.

Platinum polypyridyl complexes are attractive choices to act as the metal component. Their rich photophysical behavior[15] has been extensively studied for applications in biological sensing and photocatalysis, and in color-based sensors. The photobehavior of complexes belonging to this versatile family can be tuned by tailoring the polypyridyl ligands or by varying the ancillary ligands in the square-planar Pt(II) coordination sphere.[16] Of particular interest are the metal-to-ligand and ligand-to-ligand charge transfer (MLCT and LLCT) transitions that are commonly observed in these complexes. These absorptions occur in the visible region and result in long-lived excited states that often decay radiatively. Notably, it has been demonstrated that either functionalizing the pyridyl ligand with electron-donating substituents or coordinating aromatic alkynes to the Pt center results in significant increases in excited state lifetimes.[17−19] The enhanced excited state lifetime makes them useful as inorganic photosensitizers[20−23] because sufficiently long-lived charge-separated states can drive a variety of intermolecular electron transfer reactions.[24]

When choosing the organic photochromic component, it is difficult not to focus on the dithienylethene (DTE) architecture. This particular class of photoswitch has garnered much attention because it undergoes reversible ring-closing reactions between two isomers, each having its own opto-electronic properties, when exposed to UV and visible light (Scheme 1).[25,26] The molecular backbone is also relatively easy to modify and functionalize, and the reactions tend not to occur in the dark. In addition to pursuing systems in which the photoswitch modulates properties such as absorption, emission, or redox potential, we are interested in desiging systems in which photoswitching can control chemical reactivity and function.[27−35]

Covalently attaching the DTE backbone to Pt terpyridyl complexes is an appealing route to regulate their function as

**Received:** January 28, 2011
**Published:** May 06, 2011

  

**Scheme 1**

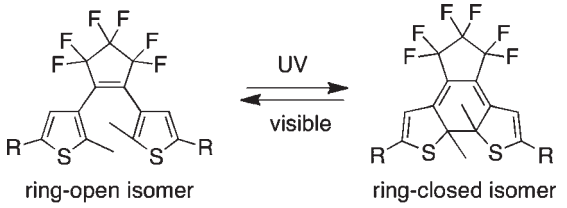


photosensitizers because the lifetime of the charge-separated excited state should depend on which isomeric form of the DTE is present. Previously, the potential of this approach was demonstrated in a bimolecular system with $[Ru(bpy)_3]^{2+}$ as the photosensitizer.[36] Covalent attachment of the photoswitch to the photosensitizer is advantageous because it strengthens the interaction between the two components. In a preliminary communication, we reported the metal-sensitized photocyclization of a DTE ligand attached to a Pt terpyridyl complex through a conjugated alkyne linker.[37] This cyclization occurs because a photoactive intraligand triplet ($^3$IL) state localized on the DTE is populated by energy transfer from triplet charge transfer ($^3$CT) states delocalized over the complex. By indirectly accessing the $^3$IL state, photoswitching can occur using light of significantly lower energy than required to directly populate the singlet excited state of the DTE. In this case of sensitized photoreactivity, the involvement of the Pt with a large spin−orbit coupling is necessary to populate the excited-state triplet manifold. This type of photobehavior is consistent with other DTE-containing Re,[38,39] Ru,[40,41] and Pt[42] complexes that also efficiently produce triplet excited states.

Despite the appeal of being able to trigger the photoreactions of DTEs in an indirect manner, this type of sensitized photocyclization is undesirable for applications involving utilization of the metal-based excited states, since these require independent excitation of the metal complex and photoswitch. One strategy to eliminate metal-sensitized photocyclization involves modifying the alkynyl linkage to electronically isolate the Pt(trpy) and DTE chromophores by introducing a nonconjugated bridge. In this article, the excited-state interactions of ligand-localized and charge-transfer states are discussed for two hybrid photoswitching systems (**1** and **2**), and are compared to those for model components **3**−**7**. Variable temperature absorption and luminescence spectroscopy, bimolecular quenching experiments, transient absorption, and DFT calculations are used to probe how the molecular architecture impacts the excited-state interactions.

## EXPERIMENTAL SECTION

**General Procedures.** All solvents and reagents including those for NMR analysis (Cambridge Isotope Laboratories) were obtained from commercial sources and used as received except where noted. $^1$H NMR spectra were recorded on a Bruker AV400-Direct (400 MHz) or Bruker AV400-Indirect (400 MHz) spectrometer. All chemical shifts are referenced to residual solvent signals, which were previously referenced to tetramethylsilane and splitting patterns are designated as s (singlet), d (doublet), t (triplet), m (multiplet), and br (broad). IR spectra were obtained on a Thermo Nicolet 6700 FT-IR spectrometer. ESI-MS (Bruker Esquire), EI-HRMS (Concept IIHQ), and elemental analysis were completed at the UBC Microanalysis facility.

**General Procedure to Prepare Pt Complexes.** A Schlenk flask was charged with [Pt(4′-tolyl-trpy)Cl]Cl, the appropriate TMS-protected acetylene, and KOH/$CH_3OH$. After sparging the reaction mixture with $N_2$ for 30 min, CuI (∼10 mol %) was added, and the reaction was left to stir under $N_2$ overnight.

Detailed synthetic procedures and characterization for complexes **1**−**4** and the ethynyl DTE precursors have been reported previously.[37,43]

**Propargyl 4-(2-Thienyl)phenyl Ether.** 4-(2-Thienyl)phenol (0.138 g, 0.789 mmol), potassium bicarbonate (0.16 g, 0.011 mol), and propargyl bromide (0.15 mL, 1.0 mmol) were dissolved in anhydrous dimethylformamide (DMF). The reaction mixture was stirred at room temperature for 20 h, at which time the product was extracted into diethyl ether and subsequently washed with $H_2O$ and brine. The organic layer was isolated, dried with $MgSO_4$, filtered, and the solvent removed in vacuo. Purification by column chromatography ($SiO_2$, hexanes/ethyl acetate 19:1) afforded 0.147 g (87%) of the title compound as a white powder. $^1$H NMR (400 MHz, $CDCl_3$) $\delta$ 2.54 (t, $J$ = 2.0 Hz, 1H), 4.73 (d, $J$ = 2.2 Hz, 2H), 7.00 (d, $J$ = 8.5 Hz, 2H), 7.06 (m, 2H), 7.22 (m, 2H), 7.56 (d, $J$ = 8.7 Hz, 2H).

**[(4′-Tolyl-trpy)Pt(C≡C−$CH_2$−O−$C_6H_4$−$C_4H_3S$)]$PF_6$ (5).** Propargyl 4-(2-thienyl)phenyl ether (0.056 g, 0.263 mmol) and KOH (0.044 g, 0.79 mmol) were added to 50 mL of $N_2$-sparged $CH_3OH$. The reaction was stirred at room temperature for 30 min after which it was treated with [Pt(4′-tolyl-trpy)Cl]Cl (0.135 g, 0.24 mmol) and CuI (0.007 g, 0.036 mmol). The reaction mixture was stirred under a $N_2$ atmosphere for 48 h at room temperature. The $CH_3OH$ was removed in vacuo leaving an orange precipitate, which was dissolved in a minimal amount of DMF and added dropwise to an aqueous solution of $NH_4PF_6$ (0.300 g in 150 mL $H_2O$). After stirring for 1 h, the resulting precipitate was filtered off and washed with $H_2O$, $CH_3OH$, and diethyl ether. The isolated orange solid was added to a solution of EtOH:$CH_3CN$ (20:1) that was heated to reflux. Any undissolved solid was filtered off yielding 0.100 g (60%) of the product, which was recrystallized by slow diffusion of diethyl ether into a $CH_3CN$ solution. $^1$H NMR (400 MHz, acetone-$d_6$) $\delta$ 2.46 (s, 3H), 5.08 (s, 2H), 7.11 (dd, $J$ = 5.1 Hz, 1H), 7.20 (d, $J$ = 8.7 Hz, 2H), 7.35 (d, $J$ = 2.8 Hz, 1H), 7.41 (d, $J$ = 5.2 Hz, 1H), 7.49

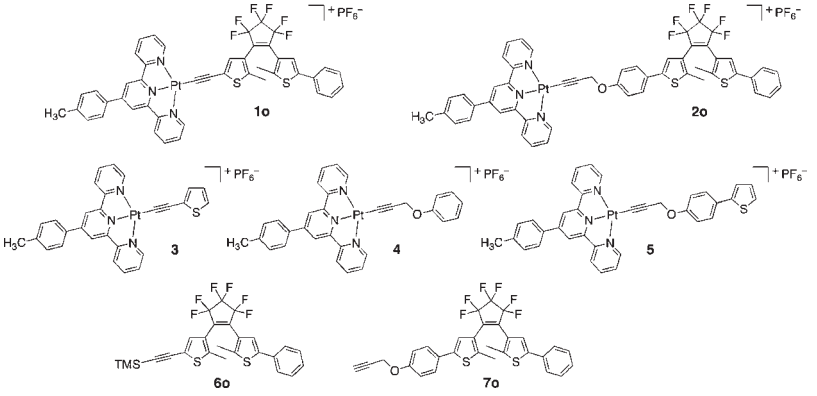



dx.doi.org/10.1021/ic200200j |Inorg. Chem. 2011, 50, 4956–4966

(d, $J$ = 8.1 Hz, 2H), 7.66 (d, $J$ = 8.7 Hz, 2H), 7.73 (t, $J$ = 6.5 Hz, 2H), 8.04 (d, $J$ = 8.1 Hz, 2H), 8.49 (t, $J$ = 7.9 Hz, 2H), 8.77 (d, $J$ = 8.3 Hz, 2H), 8.91 (s, 2H), 8.94 (d, $J$ = 5.9 Hz, 2H). ESI-MS $m/z$ 731.3 [$M^+-PF_6$]. FT-IR (solid, $cm^{-1}$): 2135 (s, $\nu_{C\equiv C}$). Anal. Calcd for $C_{35}H_{26}F_6N_3OPSPt$: C, 47.95; H, 2.97; N, 4.79. Found: C, 47.58; H, 3.10; N, 4.44.

**Photophysical Measurements.** For UV light irradiations, either an unfiltered 302 nm Hg lamp (18 mW/$cm^2$) or filtered TLC hand-lamp (UVP Model:UVGL-58) was used, unless otherwise noted. For broadband visible light irradiation, a hand-held lamp with a tungsten bulb (65 mW/$cm^2$) fitted with the appropriate low-pass filter was used. To determine the active wavelengths for photocyclization, a 75-W arc lamp with a double monochromator was used to irradiate the sample.

Samples for all spectroscopic measurements were prepared using HPLC-grade Fisher solvents, which were used as received. Absorption spectra were obtained on a Varian Cary 5000 spectrometer. Fluorescence spectra were collected on a Photon Technology International fluorimeter using a 75-W arc lamp as the source. Emission quantum yields were measured using an integrating sphere. Time-resolved emission data were collected using a Horiba Yvon Fluorocube TCSPC apparatus. A 470 nm NanoLED source pulsing at a repetition rate of 50 kHz was used for excitation. Broadband emission was monitored by a CCD detector at $\lambda$ > 500 nm, using a low pass filter. Data were fit using the DAS6 Data Analysis software package. The reported lifetimes are averages of 3 measurements. All samples for luminescence studies were prepared in $CH_2Cl_2$ that had been previously dried by passing through an alumina column and deaerated by no less than three freeze−pump−thaw cycles. Sample solutions were maintained under $N_2$ atmosphere for the duration of the experiment in 1 $cm^2$ anaerobic quartz cells (NSG PCI cells) fitted with a PTFE valve.

Quantum yields of the ring-closing reactions ($\phi_{rc}$) were obtained using a ferrioxalate actinometer to determine photon flux. Irradiations were carried out on samples dissolved in $CH_3CN$ using a 75-W arc lamp as the source, with a double monochromator to isolate the desired wavelength (425 or 302 nm). Full details of the calculations are given in the Supporting Information.

Transient absorption experiments were performed using a Nd:YAG laser (EKSPLA PL2241) that generated pulses of 35 ps (fwhm) in duration. The third harmonic output (355 nm) was employed as the pump beam. The fundamental, 1064-nm output pumped a Xe-filled quartz cell to generate the white light continuum used as the probe beam. The pump and probe beams were aligned to pass through the sample at a 90° angle and focused so that the probe beam was completely enclosed by the pump beam within the cuvette. The probe beam was detected by first passing through a monochromator (Princeton Instruments SpectraPro 2300i) equipped with a 150 g/mm diffraction grating. The grating was centered at 470 nm, 540 nm, or 640 nm to collect data over the 350−800 nm spectral region. This was coupled to a streak camera (Hamamatsu C7700) and a CCD detector (Hamamatsu C8484), which digitized the images from the streakscope. The trigger delay between the streak camera and the pulse firing was controlled using a passive delay unit (Hamamatsu C1097−01). Computer control of data acquisition was via HPD-TA software (ver. 8.3) from Hamamatsu. The data consists of a 200-shot average. Samples for transient absorption were prepared in HPLC grade $CH_3CN$ (Fisher) that had been previously deaerated by three freeze−pump−thaw cycles and were maintained under a $N_2$ atmosphere for the duration of the experiment. Steady-state UV−vis absorption spectra were collected before and after laser photolysis to confirm sample degradation was not significant during the course of the experiment.

**TDDFT and DFT Calculations.** ADF 2007.01[44,45] all-electron calculations were performed with TZ2P basis sets, scalar relativistic effects included through the ZORA[46−48] formalism and solvation effects ($CH_2Cl_2$) through the COSMO[49] formalism. Geometry optimizations were carried out with the Becke-Perdew GGA potential and time-dependent density functional theory (TDDFT)[50,51] calculations of electronic transitions with the SAOP model potential.

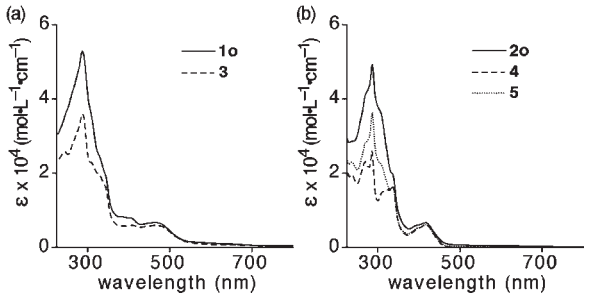


**Figure 1.** UV−vis absorption spectra of $CH_3CN$ solutions of (a) complexes **1o** and **3**, and (b) complexes **2o**, **4**, and **5**.

## RESULTS AND DISCUSSION

**Ground State Electronic Absorption Properties.** The absorption spectra of the ring-open form of each of the photochromic DTE-Pt complexes (**1o** and **2o**) and the comparative spectra of the respective model complexes that do not contain the DTE components (**3**, **4** and **5**) are shown in Figure 1. The absorption spectra of Pt terpyridyl complexes typically originate from two sets of transitions. The higher energy $\pi\rightarrow\pi^*$ transitions involve ligand-localized orbitals of the terpyridine and acetylide ligands. The lower energy transitions arise from charge transfer transitions from orbitals that have significant mixing of metal and acetylide ligand character to low-lying $\pi^*$ orbitals localized on the terpyridine.[16,19] Conjugation of aromatic groups directly to the acetylide group increases the participation of the alkynyl ligand in the CT transitions. Strongly electron-donating ligands give rise to CT transitions that are more ligand-to-ligand in nature and occur at lower energies than in cases where the highest occupied molecular orbital (HOMO) primarily involves the metal atom. This accounts for the lower energy CT absorptions in **1o** and **3** compared to **2o**, **4**, and **5**. Throughout this article, we generally refer to those transitions that have both MLCT and LLCT character as CT transitions. A comparison of the spectroscopic properties of the Pt complexes is summarized in Table 1.

In the UV region of the spectrum, both photochromic complexes have higher molar absorptivities because of the presence of DTE-localized thiophene-based $\pi\rightarrow\pi^*$ transitions which are absent in the model compounds. The nearly identical molar absorptivities of the lowest energy bands, which are assigned to charge transfer transitions in the DTE and model complexes, are indicative that these transitions do not significantly involve the whole photoswitch component. A comparison of the absorption spectra of hybrid system **1o** to its model **3** demonstrates that the lowest energy CT transitions of the complexes are not perturbed by the presence of the DTE component. The CT bands for the ether-linked complexes **2o**, **4**, and **5** appear between ~380−450 nm, which are blue-shifted significantly from the corresponding bands in **1o** and **3**. The lowest unoccupied molecular orbital (LUMO) energies are expected to be similar for all the complexes, so these trends are attributed to differences in the HOMO energies. Notably, the CT bands in complexes **4** and **5** are similar suggesting that the HOMOs are the same in these complexes, and are localized on the metal acetylide moiety with little influence of the aromatic groups located on the distal

**Table 1. Spectroscopic Data for Compounds 1−5**

| compound | abs $\lambda_{max}$ (nm)[a] | Em $\lambda_{max}$ (nm) | $\tau_{em}$ ($\mu$s)[c] | $\phi_{em}$[c] | $\phi_{rc}$[a] |
|---|---|---|---|---|---|
| **1o** | 287, 383, 404, 465 | 568, 608[b] | | | 0.14 ± 0.02,[d] 0.41 ± 0.07[e] |
| **1c** | 266, 286, 310, 328, 382, 404 (sh), 602 | | | | |
| **2o** | 286, 336 (sh), 396 (sh), 417 | | | | 0.03 ± 0.004[d] |
| **2c** | 268, 286, 314, 336, 380, 416, 592 | | | | |
| **3** | 288, 384, 409, 466 | | | | |
| **4** | 286, 336, 396 (sh), 418 | 548, 582 (sh)[c] | 2.92 ± 0.006 | 0.076 ± 0.003 | |
| **5** | 286, 336, 396 (sh), 418 | 558[c] | 3.50 ± 0.012 | 0.048 ± 0.003 | |

[a] At room temperature in $CH_3CN$ solution. [b] At 90K in EtOH:MeOH (4:1) glass. [c] At room temperature in $CH_2Cl_2$ solution. [d] $\lambda_{ex}$ = 425 nm. [e] $\lambda_{ex}$ = 302 nm.

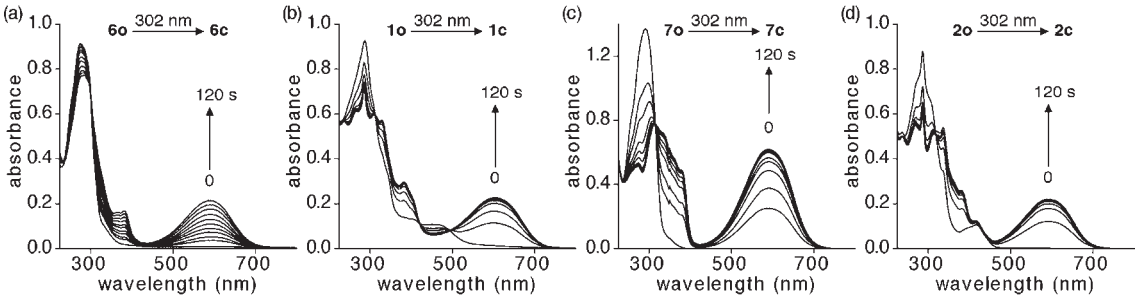


**Figure 2.** Changes in the absorption spectra of $CH_3CN$ solutions of (a) **6o**, (b) **1o**, (c) **7o**, and (d) **2o** upon irradiation with 302 nm light.

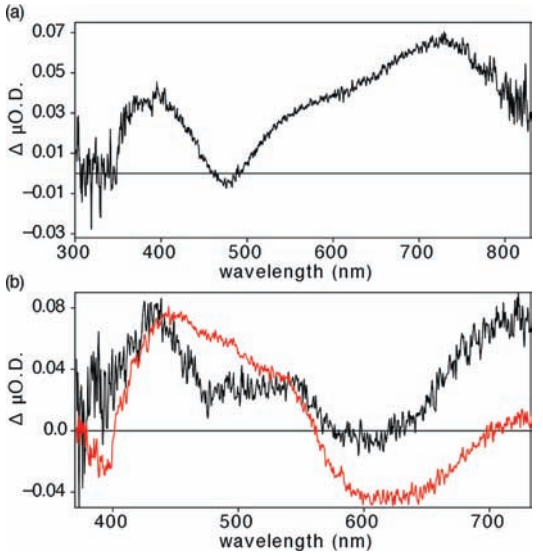


**Figure 3.** Transient absorption difference spectra for $CH_3CN$ solutions of (a) **3** and (b) **1o** (black) and **1c** (red) measured in at 800 ps following a 355 nm laser pulse.

end of the nonconjugated linkage. This is also consistent with the changes observed in the absorption spectra upon ring-closing of the appended DTE components in hybrid systems **1o** and **2o**. In **1o**, where the DTE is attached through a conjugated linker, the CT bands red-shift upon conversion of the DTE to the ring-closed form (**1c**) supporting the presence of ground-state interaction of the metal complex and the photoswitch (Figure 2b). This behavior contrasts with that of complex **2**, where no shift of the CT bands is observed when **2o** is converted to **2c** (Figure 2d). The increase in absorption from 300−400 nm upon photocyclization of **1o** and **2o** is assigned to localized DTE transitions by comparison to the absorption spectra of **6o** and **7o** (Figure 2).

**Excited-State Interactions Involved in Metal-Sensitized Ring-Closure.** In our recent report describing the metal-sensitized photocyclization of DTE photoswitches, we highlighted that visible light irradiation of the Pt sensitizer induces the ring-closing reaction, and that the two components (the metal complex and the DTE) must be covalently linked through a conjugated pathway for this to occur.[37] Here we present a detailed understanding of the excited-state interactions between the two components that lead to the visible light-sensitized ring-closing. The transient absorption (TA) difference spectra of complexes **1o**, **1c**, and **3** measured at various delay times after excitation at 355 nm are shown in Figure 3. The TA spectrum of the model complex **3** shows a bleach in the region between 450−500 nm between strong positive absorption bands at higher and lower energies (Figure 3a). This bleach is coincident with the ground state absorption bands assigned to the CT transitions. The broad, positive absorption at lower energy clearly consists of at least two overlapping bands and is similar to the TA spectrum of the phenyl acetylide complex.[52] On the basis of excited-state spectra of other Pt terpyridyl complexes,[53] we assign the absorption bands centered at 540 and 690 nm to transitions in the transiently formed terpyridyl anion and the band at 400 nm to transitions in the transient cation localized on the metal acetylide. The transient signal of complex **3** decays simultaneously over the wavelength range with a lifetime $\tau$ = 8 ns (Supporting Information, Figure S1).

Excitation of the hybrid system **1o** with 355 nm light results in photocyclization of the DTE photoswitch either by direct excitation or through energy transfer from the metal-based CT states; however, these two processes occur on significantly different time scales. Whereas direct excitation of the DTE is expected to result in photocyclization within picoseconds,[54]


dx.doi.org/10.1021/ic200200j |Inorg. Chem. 2011, 50, 4956–4966

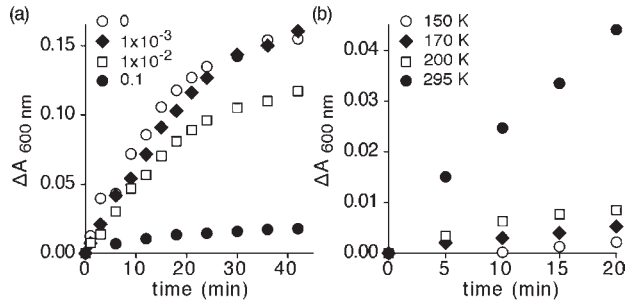


**Figure 4.** (a) Changes in absorbance at $\lambda$ = 600 nm of $CH_3CN$ solutions of **1o** ($1.4 \times 10^{-5}$ M) without quencher (○) or with varying concentrations of DABCO, $1.0 \times 10^{-3}$ M (♦), $1.0 \times 10^{-2}$ M (□), and 0.10 M (●), upon irradiation with light of wavelengths greater than 420 nm. (b) Changes in absorbance at $\lambda$ = 600 nm when an EtOH:$CH_3OH$ solution of **1o** is irradiated with light of wavelengths greater than 420 nm at 150 K (○), 170 K (♦), 200 K (□), and 295 K (●).

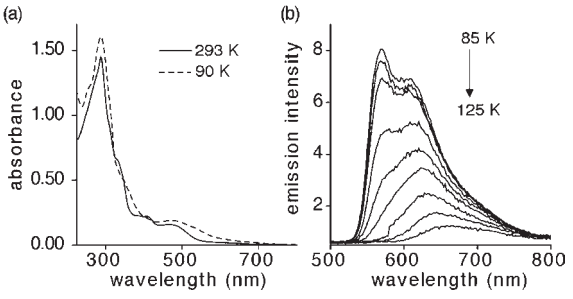


**Figure 5.** UV−vis absorption spectra (a) and changes in emission spectra (b) when an EtOH:$CH_3OH$ (4:1) glass of hybrid complex **1o** is warmed from 85 to 125 K. Excitation = 470 nm.

energy transfer processes occurring within the triplet manifold are more likely to occur on a time scale on the order of tens of nanoseconds.[39] In this experiment, a fresh sample was continuously passed through a flow cell; however, accumulation of the ring-closed form of the system (**1c**) in the beam path still occurred. The bleach centered at 600 nm is indicative of some accumulation of **1c**, based on comparison to the TA spectrum of **1c**, produced directly by 355 nm excitation. There are, however, some notable excited state spectral differences between the hybrid system **1o** and the model compound **3**. The TA spectrum of **1o** does not exhibit a bleach overlapping with the ground state CT absorption, and the positive absorption at ~430 nm is considerably red-shifted compared to its counterpart in **3**. This spectrum is assigned to the $^3$IL state of the DTE, which must form faster than the time resolution of the instrument since this was the only signal observed.

The TA spectrum observed after excitation of the ring-closed isomer **1c** is notably different than that observed for its ring-open counterpart (**1o**) or model compound **3** (Figure 3b). An intense bleach appears between 560−700 nm, the spectral region that coincides with the $\pi \rightarrow \pi^*$ absorption of the ring-closed DTE. Cyclization of the photoswitch results in the HOMO becoming predominantly localized on the DTE component and consequently the lowest energy absorptions are ascribed to LLCT transitions. The positive absorption appearing in the TA spectrum of ring-closed **1c** is slightly red-shifted compared to **1o**. It is unclear whether this feature is more appropriately assigned to the $^3$LLCT state or the $^3$IL state of the photocyclized DTE. The transient signal of complex **1c** decays simultaneously over the wavelength range with a lifetime $\tau$ = 10 ns (Supporting Information, Figure S2).

Recently, Castellano and co-workers demonstrated that 1,4-diazabicyclo-[2.2.2]octane (DABCO) efficiently reduces the transient hole localized on the Pt atom and aryl acetylide ligand in the charge-separated excited state of several Pt terpyridyl complexes.[53] DABCO is a suitable reductive quencher since it does not absorb in the spectral region where the Pt complex is excited. We used this bimolecular quenching reaction as a means to provide further evidence for the existence of a charge-separated state involved in the photosensitized ring closure of **1o**. The rate of photocyclization (**1o**→**1c**) by irradiation with light of wavelengths greater than 420 nm was monitored over time with various concentrations of DABCO (Figure 4a). Formation of the ring-closed isomer (**1c**) was evident by the increased absorbance at 600 nm, where only **1c** absorbs. In the ring-open isomer (**1o**) the charge-separated state that is formed initially after excitation transfers its energy to the DTE component, so efficient quenching of the charge-separated state with DABCO is expected to prevent sensitized photocyclization.

At sufficiently high concentrations of DABCO, diffusion-controlled quenching of the excited state of **1o** occurs when irradiating with visible light, as evidenced by suppression of the cyclization of **1o** to produce **1c**. In this case, the rate of intermolecular reductive quenching is faster than the rate of intramolecular energy transfer to the DTE component. At a 0.10 M DABCO concentration, quenching almost completely suppresses photocyclization of the photoswitch. Significantly, irradiation of this solution with UV light results in direct excitation of the DTE component and **1o** photocyclizes at a comparable rate to that when quencher is not present. This observation demonstrates the difference in the rate of photoswitching with respect to the excited state pathways following excitation with visible light or UV light. The metal-sensitized ring closure, initiated by visible light excitation, is a slow excited-state process, occurring on the nanosecond time scale, and is susceptible to intermolecular quenching. Irradiation with UV light excites the DTE directly, resulting in fast (picoseconds) photocyclization of the DTE core.

The rate of energy transfer was also reduced by cooling the system to lower temperature. An EtOH:$CH_3OH$ (4:1) solution of **1o** was frozen to a glass at 85 K. Photocyclization of **1o** was monitored by measuring the changes in absorbance at 600 nm corresponding to the appearance of ring-closed **1c**. At 85 K, irradiation with light of wavelengths greater than 420 nm does not result in an appreciable amount of **1c** being formed after 20 min of irradiation (Figure 4b). Warming the glass through its melting point (130−150 K), results in the onset of cyclization of **1o** and the appearance of **1c**. Raising the temperature further resulted in an increase in the rate at which photocyclization occurred. It is important to note that **1o** is photoactive at temperatures down to 90 K when irradiated with UV light. This confirms that the DTE is still photoactive in the frozen matrix, eliminating the restriction of rotation as an explanation for the lack of visible light-induced photocyclization below 130 K.

The observed temperature dependence of photoactivity with UV or visible light irradiation further supports the conclusion that there are at least two separate excited state pathways that lead to photocyclization of **1o**. Irradiation with UV light results in direct population of the photoactive excited singlet state of the DTE component. In solution, the photoswitch in **1o** adopts two conformations. When in the antiparallel conformation,[55,56] in

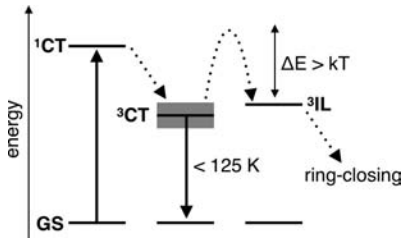


**Figure 6.** Proposed Jablonski diagram rationalizing the low temperature emission of hybrid complex **1o**. The shaded box represents limits on the energy of the $^3$CT state.

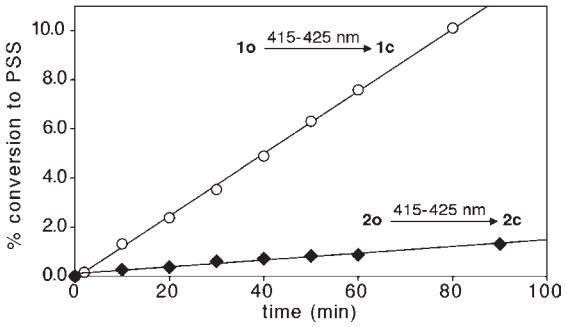


**Figure 7.** Percent conversion to the photostationary states as a function of time for $CH_3CN$ solutions of **1o** and **2o** when irradiated at wavelengths between 415 and 425 nm. Linear fits are shown.

which the orientation of the thiophene rings results in a $C_2$ symmetric conformation with the reactive carbons of each thiophene in close proximity to each other, ring-closing occurs. Upon freezing, a small amount of reorganizational energy is required for the conversion of **1o** to **1c** compared to if the photoswitch was frozen in the photoinactive parallel conformation (the orientation of the thiophene rings results in a mirror plane) and required interconversion to the photoactive antiparallel conformation. This fact accounts for its photoactivity at low temperatures when irradiated with UV light. On the other hand, photocyclization of **1o** with visible light, via intramolecular energy transfer, occurs by a pathway with additional energy barriers and competing deactivation pathways (such as phosphorescence). Energy transfer from the $^3$CT to the $^3$IL state requires sufficient thermal energy to overcome the barrier between states. DFT calculations estimate that in the ring-open complex (**1o**), the DTE $^3\pi\rightarrow^3\pi^*$ orbital energy difference (localized on the remote acetylene-thiophene moiety) that leads to ring closing is only 0.02 eV higher than the lowest $^3\pi\rightarrow^3\pi^*$ orbital energy difference localized on the adjacent acetylide moiety. At room temperature sufficient thermal energy is present to populate the $^3$IL state capable of photocyclization. Below 140 K, the cyclization reaction no longer occurs, likely because there is no longer sufficient thermal energy to populate the $^3$IL state that leads to ring closing.

An important result correlated to the suppression of photoactivity at low temperature is that strong emission is observed from complex **1o** (Figure 5b) below 125 K. The spectral profile of the orange emission is characterized by multiple peaks with well-defined vibronic spacing of approximately 1200 $cm^{-1}$ attributed to the ring "breathing" of the terpyridyl scaffold. Comparison of the energy and vibronic spacing to other Pt terpyridyl acetylide complexes strongly supports the conclusion that the emission originates from a state localized on the Pt terpyridine moiety.[18,52] As the temperature is increased closer to the melting range of the glass, the emission profile becomes less structured and intense until it completely disappears at temperatures above 125 K.

The efficiency of energy transfer is governed by the energy gap between donor and acceptor energy levels, and by the height of the energy barrier that exists between them.[57] The diminished thermal energy available at low temperatures might not be enough to overcome the energy barrier between the $^3$CT and $^3$IL states (Figure 6). Although the $^3$IL excited state may still lie at an accessible energy level near the $^3$CT state, the energy barrier forces deactivation from the $^3$CT state, which is characterized by orange phosphorescence. Additionally, examination of the absorption spectrum at low temperature reveals transitions at lower energies than those at room temperature (Figure 5a). The appearance of these lower energy transitions suggests that CT states might lie at lower energies at low temperature. A change in the relative energies of the $^3$CT and the $^3$IL states would affect the rates of energy transfer between them, resulting in radiative decay from the $^3$CT state as the primary pathway of excited-state deactivation rather than energy transfer to the ligand (Figure 6). The most likely scenario is that contributions from both the adjustments in the relative energies of the excited states and the contributions of thermal energy play a role in the photophysical behavior at low temperature.

**Excited-State Interactions for the Ether-Linked System.** Hybrid complex **2o** was designed with the intent to limit the interactions of the $^3$CT and $^3$IL states. In addition to conventional ring-closing of the DTE component in **2o** using UV light, cyclization is also triggered with selective irradiation into the MLCT band in this complex. Although this photobehavior is similar to that of complex **1o**, it is clear that there is a significant difference in the efficiency of photocyclization using visible light. To compare the relative efficiencies of ring-closing when excited with visible light, solutions of complexes **1o** and **2o** were irradiated under the same conditions with light between wavelengths 415 and 425 nm.

The progress of the photoreactions was monitored by UV−vis spectroscopy. To ensure each sample absorbed the same number of photons, the solutions were prepared with absorbances greater than 2.5 at the irradiation wavelength so that the majority of light was absorbed by both samples. Conversions of the DTE components to their ring-closed isomers were kept below 10% for both samples so that absorbance by the ring-closed isomers does not interfere significantly with the cyclization photoreaction. The amount converted to the ring-closed form was determined by calculating the ratio of absorbance at either 602 nm (**1o**) or 592 nm (**2o**) relative to the absorbance at 286 nm after each time interval of irradiation. The ratios at various time intervals were then divided by the same ratio, representative of the total changes in the samples, to give the percentages photocyclized of the total amounts achievable at the photostationary states. The relative rates of both photoreactions (**1o**→**1c** and **2o**→**2c**) are illustrated in Figure 7. Clearly, system **1o** demonstrates more efficient photocyclization using visible light and although ring-closing is not completely quenched for **2o**, it is evident the linkage has a substantial effect. The difference in rate is also reflected in the larger ring-closing quantum yield for compound **1o** (Table 1) than that for compound **2o**. The fact that the quantum yield is smaller for **1o** when 425 nm light is used than when 302 nm light


dx.doi.org/10.1021/ic200200j |*Inorg. Chem.* 2011, 50, 4956–4966

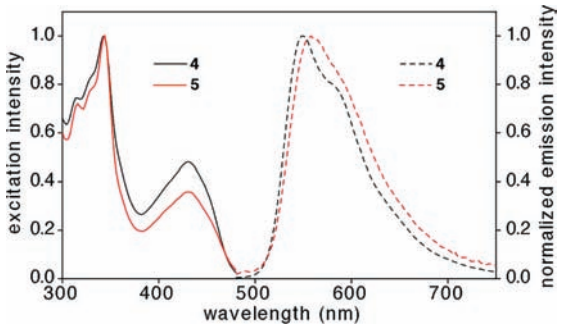


**Figure 8.** Corrected emission (dashed line) and excitation (solid line) spectra for $CH_2Cl_2$ solutions of complexes **4** (black) and **5** (red). Emission spectra were collected by exciting the solutions at 425 nm. Excitation spectra were collected by monitoring emission at 550 nm for complex **4** and 560 nm for complex **5**.

is used is a consequence of the presence of additional pathways for decay of the $^3$CT state involved in the indirect ring-closing.

The lower efficiency of sensitized ring-closing of **2o** compared to **1o** suggests that other pathways are involved in its excited-state decay. The model complexes **4** and **5** generally exhibit the same structured emission, where both the wavelength and band shape of emission are characteristic of Pt terpyridyl $^3$MLCT-based phosphorescence (Figure 8). Since there is virtually no effect on the emission, regardless of how the alkynyl ligand is terminated, it appears that the CT state for these complexes involves transfer of an electron from a mixed Pt-alkynyl orbital to a low-lying terpyridyl $\pi^*$ orbital. This interpretation is also supported by the excitation spectra, which are identical to the respective absorption spectra for the respective complexes. Comparatively weak emission was detected for $CH_2Cl_2$ solutions of complex **2o** or **2c** relative to the model compounds. Despite no indication that **2** was impure in the characterization data (NMR or elemental analysis), this emission was determined to at least partly originate from trace $[Pt(trpy)Cl]PF_6$ by comparison of the excitation spectrum with the absorption spectrum of **2o**. Therefore, emission from neither complex **2o** nor **2c** was conclusively established.

The excited-state lifetimes and fluorescence quantum yields for complexes **4** and **5** are listed in Table 1. The emission decay profiles for both complexes were fit to monoexponential models (Supporting Information, Figure S3), supporting the conclusion that only one excited state was responsible for the observed emission in each case. Their excited-state lifetimes are both on the order of a few microseconds, a result consistent with the notion that the same emitting state is responsible for emission. The complexes also exhibit similar emission efficiency. Complex **4** has a slightly higher quantum yield than **5**.

Given the slight differences in the lifetimes and quantum yields, there are several possible interpretations of these data. Minor differences might result because varying the substitution on the alkynyl ligand could perturb the $^3$MLCT relaxation processes differently. Alternatively, additional states may be present, depending on how the alkynyl ligand is substituted, that could be accessible or interact with the emitting $^3$MLCT state. The aromatic groups incorporate low-lying $^3$IL states that could be populated by energy transfer from the $^3$MLCT state. For instance, this would be expected comparing **4** to **5**, where extension of the conjugated backbone and addition of thiophene (which often has a low-lying nonemissive triplet state) is consistent with the notion that

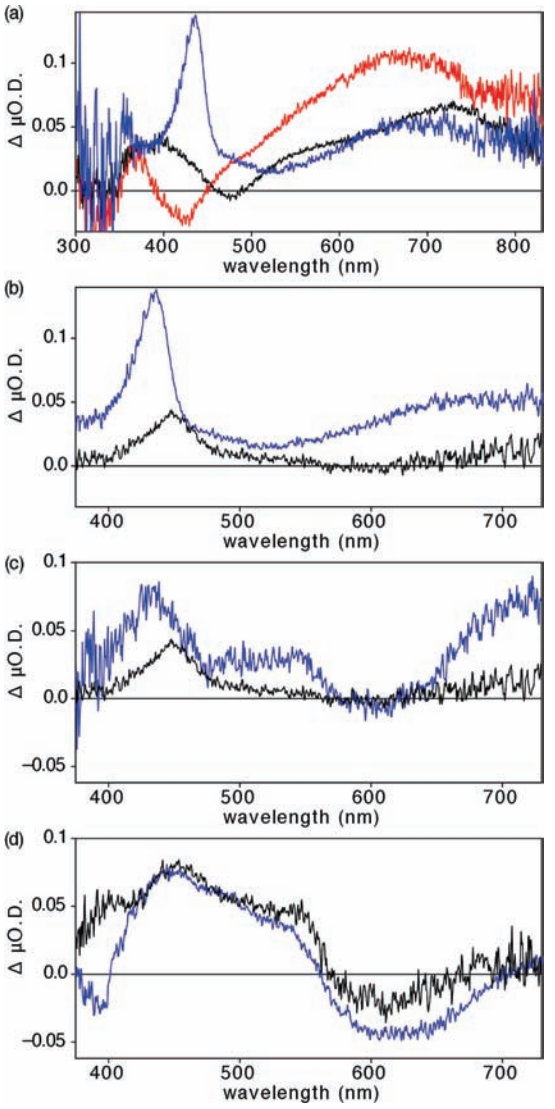


**Figure 9.** Transient absorption difference spectra of $CH_3CN$ solutions of (a) complexes **3** (black), **4** (red), and **5** (blue), (b) complexes **2o** (black) and **5** (blue), (c) complexes **1o** (blue) and **2o** (black), and (d) complexes **1c** (blue) and **2c** (black). All data were collected at 800 ps after excitation at 355 nm.

lowering of a $^3$IL state could funnel energy from the emissive $^3$MLCT state. If a $^3$IL state were populated, the observed decay for the excited-state species would be dependent on the relative rates of relaxation from either the $^3$MLCT or the $^3$IL states and the rates of energy transfer between them. The differences in rates would account for some fluctuation in the excited-state lifetime and quantum efficiency. This would explain the appearance of emission from the same $^3$MLCT state, with slightly perturbed dynamics affected by the substitution of the alkynyl ligand.

The transient absorptions of the excited state species of the complexes were measured by picosecond pump−probe laser spectroscopy to further elucidate the excited state dynamics of the complexes. Upon excitation of complex **4** at 355 nm, the resulting transient species has a similar spectral profile to the directly linked thienyl model complex **3** (Figure 9a). The difference spectrum of **4** is characterized by a positive absorption centered at 365 nm, a bleach from 390−450 nm, and a broad,

**Scheme 2**

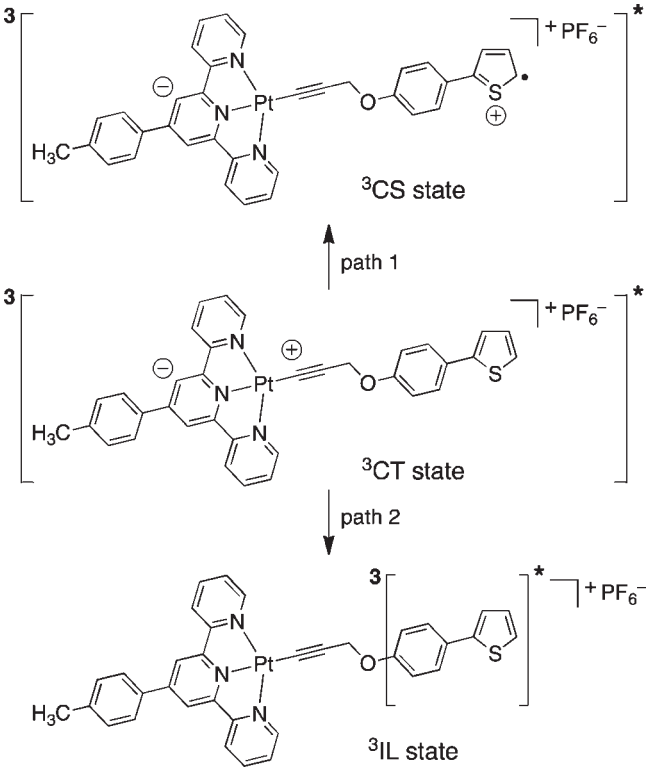


intense positive absorption throughout the visible region greater than 450 nm. The appearance of a bleach coinciding with ground state CT absorption, and its similarity to spectra observed for other Pt terpyridyl complexes, provides strong supporting evidence that this spectrum originates from the $^3$MLCT state. The transient signal decays monoexponentially at all wavelengths with $\tau$ = 6.3 ns (Supporting Information, Figure S4).

Despite having nearly identical ground state absorption spectra and similar emission profiles, the TA difference spectra for complexes **4** and **5** indicate different excited-state behavior. The difference spectra measured at 800 ps after 355-nm excitation for $CH_3CN$ solutions are shown in Figure 9a. For complex **5**, an intense, positive absorption centered at 440 nm appears in the region coinciding with the bleach observed for complex **4**. The positive absorption that appears at lower energy for **5** is consistent in band shape and energy with that for **4**. Comparing the absorbance decay absorption from 650−680 nm, complex **5** exhibits a shorter lifetime than **4**, $\tau$ = 2.0 ns compared to $\tau$ = 6.3 ns, respectively (Supporting Information, Figures S4 and S5).

The assignment of the transient signal for **5** is complicated by the nature of a difference spectrum, for which the data may be a combination of signals of different signs. As such, concurrent overlapping positive and negative changes can mask the appearance of one or the other based on their relative intensities. With this in mind, there are two possible states to which the observed signal could be attributed (Scheme 2). The spectrum could be assigned as a charge-separated state ($^3$CS) with the cation localized over the phenyl and thienyl rings instead of the Pt-acetylide unit (the $^3$CT state). This would account for the bathochromic shift and change in band shape of the absorption band attributed to the cation relative to complex **4**. Since this band coincidentally overlaps with the ground state CT absorption, a bleach does not appear as it does in the spectrum of **4** because the concurrent positive absorption is more intense. Despite the alteration of the spectrum attributed to the transient cation, the appearance of the lower energy band corresponding to the terpyridyl-localized anion remains unchanged compared to **4**. If direct excitation resulted in ligand-to-ligand charge transfer, one would expect this difference to manifest itself in the ground-state absorption spectra, for which **4** and **5** are identical in terms of their CT absorptions. Therefore, the formation of this state would likely be a two-step process similar to the behavior of the Pt chromophores reported by Eisenberg and designed to undergo photoinitiated electron transfer cascades.[52,58] Within the limitations of the picosecond TA experimental setup, however, the excited-state species responsible for this transient spectrum shown in Figure 9a is the only one observed.

The other explanation is that the signal arises from a $^3$IL state localized on the phenyl-thiophene subunit, shown as "path 2" in Scheme 2. DFT calculations estimate that with the addition of the thiophene in complex **5**, the $^3$IL state falls considerably ($\approx$ 1 eV) in energy relative to **4**. The lowering of the $^3$IL state could make it accessible from the $^3$MLCT state. These two excited states could be in equilibrium, which would explain the appearance of $^3$MLCT-based emission in the spectrum of **5**. The nearly identical ground state absorption spectra and similar phosphorescence of complexes **4** and **5** support that the same excited state is responsible for radiative decay in all of those complexes. The appearance of the $^3$IL state in the transient spectrum and emission from the $^3$MLCT state is consistent with observations for other metal complexes with approximately isoenergetic $^3$MLCT and $^3$IL states.[59] The excited-state lifetime is not, however, observed to be significantly longer as one might expect if the two states were in equilibrium.[17,60,61] It is possible that the rate of decay from the $^3$IL state is comparable to that of the $^3$MLCT state and therefore there is no enhancement of excited-state lifetime. The ability to populate the $^3$IL state in complex **5** would be supporting evidence that a low-lying $^3$IL state exists within the molecular linker and could act as a conduit to a $^3$IL state responsible for Pt-sensitized photocyclization of the DTE component.

To acquire a TA spectrum for the excited state species of **2o**, fresh sample solution was continuously pumped through a flow cell to prevent buildup of the photoproduct **2c** in the probe beam. Although 355-nm excitation addresses both the CT transition and the photoswitch directly, the photoactive $^1\pi^*$ DTE state, which is only accessible by direct UV excitation, is assumed to have completely decayed within tens of picoseconds, an assumption supported by other work.[54] Therefore, the transient signal observed on the nanosecond time scale is interpreted as being directly related to the excited-state dynamics resulting from excitation of the CT transition.

The TA spectra for complexes **5** and **2o** are similar (Figure 9b). A positive absorption appears centered at 450 nm, red-shifted 15 nm from the similar absorption observed for **5**. Fitting the decay of this absorption to a monoexponential model indicates similar lifetimes ($\tau$ = 2.4 ns for **2o** and $\tau$ = 1.4 ns for **5**) for the two excited-state species (Supporting Information, Figures S5 and S6). The very shallow bleach centered at 600 nm is attributed to the accumulation of some **2c** (Figure 9d) in the sample beam despite being replenished continually in the flow cell. The bleach appears to diminish the intensity of a coincident positive absorption that would be consistent with the spectrum appearing

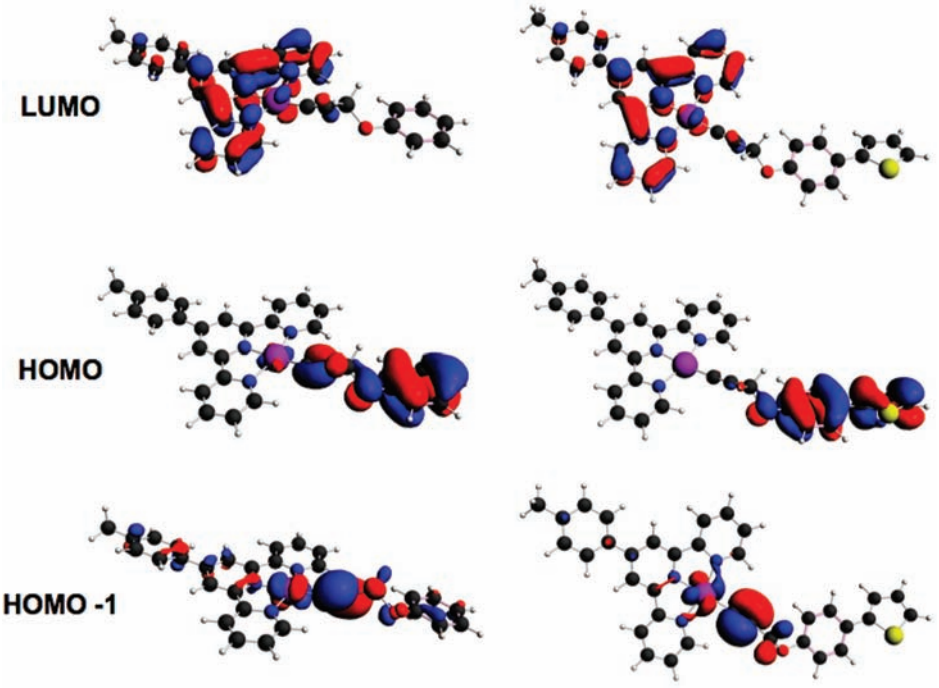


**Figure 10.** Contour plots of the LUMO, HOMO, and HOMO-1 for complexes **4** (left) and **5** (right).

for **5**. Therefore, our interpretation is that this excited-state absorption is attributed to the same state for both **5** and **2o**. Evidence that these spectra might be attributed to a $^3$IL state is found by comparison to the TA signal observed for **1o** (Figure 9c). Although the positive absorption exhibited by **2o** is slightly red-shifted compared to that observed for **1o**, the similar band shape and spectral features that appear throughout the visible region suggest that these features originate from the same state. For hybrid system **1o**, the intense bleach centered at about 600 nm is indicative of accumulation of the ring-closed isomer (**1c**). Assignment of this signal as a $^3$IL state is consistent with the observed photoswitching behavior of **2o**, which undergoes ring-closing with lower energy light when coordinated to the Pt complex than when not coordinated.

A comparison of the TA spectra for $CH_3CN$ solutions of **1c** and **2c** is shown in Figure 9d. The essentially identical spectra support that the same state is populated by excitation of either complex. The only excited state in common between **1c** and **2c** that should generate the same spectral signature is the DTE-localized $^3$IL state. Additionally, the comparable excited-state lifetimes ($\tau$ = 10 ns for **1c** and $\tau$ = 8.8 ns for **2c**) support the assignment of these spectra as originating from the same excited state (Supporting Information, Figures S2 and S7). The TA spectrum of the DTE-localized $^3$IL state is characterized by an intense bleach coinciding with the ground state $\pi \rightarrow \pi^*$ absorption of the ring-closed DTE. This is accompanied by a positive absorption appearing at higher energy. The traces shown in Figure 9d represent the only spectral signature observed within the time resolution of our experimental setup. Considering that the ring-closed isomer of the DTE component exhibits appreciable absorption at 355 nm (Figures 2a and 2c), one possibility is that direct excitation of the $^1$IL state is followed by rapid intersystem crossing to the $^3$IL state, a process facilitated by the spin−orbit coupling of the appended Pt atom. Although not observed, it cannot be discounted that the $^3$CT state could be populated first, have a short lifetime, and subsequently lead to population of the $^3$IL state.

DFT and TDDFT calculations were carried out to aid in understanding the distribution of electron density and the orbitals involved in the lowest energy CT transitions. Contour plots of the LUMO, HOMO, and HOMO-1 are shown in Figure 10.

Since the lowest energy transitions that appear in the absorption spectra of complexes **2o**, **4**, and **5** are identical, the orbitals involved in those transitions must be similar. The contour plots show the orbitals relevant to the lowest energy transition. Since the majority of the electron density of the HOMO is located on the aromatic rings, which are distorted out of the Pt terpyridyl plane, the oscillator strength of the HOMO to LUMO transition is diminished. The next lowest allowed transition from HOMO-1 to LUMO is more favorable and occurs more efficiently. The similarity of the HOMO-1 and LUMO of complexes **4** and **5** supports the nearly identical CT absorption bands observed for these complexes.

Since the lowest $^3$CT energy of **2o** is comparable to that of **1o**, there should be sufficient energy to populate the $^3$IL state if energy transfer is possible. DFT calculations of the CT energies, together with observed absorption spectra of **1o** and **2o**, indicate CT energies to be $\geq$2.0 eV, in agreement with experimental and DFT-calculated values for related compounds.[62] The triplet energy of the DTE photoswitch state that leads to ring-closing is estimated from DFT calculations to be about 1.9 eV for **1o** and 1.8 eV for **2o**, values that are in good agreement with an experimental value of 1.85 $\pm$ 0.16 eV for the same photoswitch in a related Ru(II) complex.[40]

For the model complexes **4** and **5**, the trends of DFT-calculated energies for their alkynyl-ligand-based $^3$IL states are consistent with the differences observed in their luminescence behavior and TA spectra. These empirical differences have been attributed to the changes in the relative energies of the $^3$CT and


dx.doi.org/10.1021/ic200200j |*Inorg. Chem.* 2011, 50, 4956–4966

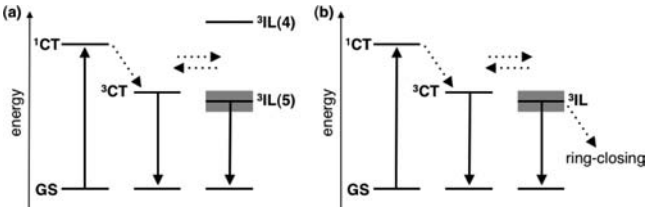


**Figure 11.** Proposed Jablonski diagrams comparing the excited-state interaction of the $^3$CT state and varying $^3$IL states for complexes (a) **4** and **5** or (b) **2o** after excitation of the CT transition. The shaded box represents limits on the energy of the $^3$IL state.

$^3$IL states, which interact with each other if they are close enough in energy. Whereas the energy of the $^3$CT state remains relatively constant for the models, the energy of the $^3$IL state drops considerably based on the functionality of the alkynyl ligand. The estimated values of the $^3$IL state energy for complexes **4** and **5** are 3.2 and 2.5 eV, respectively. If the $^3$IL state is accessible from the $^3$CT state, it might act as an alternate pathway for decay. Otherwise, emission from the $^3$CT state is the predominant decay pathway. This model is summarized in the Jablonski diagram shown in Figure 11a.

Unlike in the directly linked system **1o**, the nonconjugated, ether linkage seems to largely remove interactions between the two chromophores in the ground state. This is supported by the lack of any significant shifts of absorption bands in **2o** compared to the model complexes of its constituents. In addition, there are no shifts observed in the $^1$H NMR resonances of the DTE upon coordination, as were observed for **1o**. TDDFT-calculated oscillator strengths for transitions between the Pt and the DTE moiety in **2o** compared to **1o** (e.g., $f < 0.001$ for **2o** vs $f > 0.1$ for **1o**) are indicative of the diminished orbital overlap of the two components when linked by the nonconjugated ether linkage. Observation of the $^3$MLCT-based emission for the models is consistent with the reduced interaction between the chromophores, as opposed to efficient energy transfer to a $^3$IL state as observed in **1o**. The transient absorption data, however, show that interactions between the two chromophores exist in the excited state. DFT calculations support a model in which lowering of the $^3$IL state permits its population from the $^3$MLCT state. Population of a $^3$IL state also explains the ring-closing observed for **2o** when selectively exciting its MLCT absorption. An energy diagram for **2o** illustrating the proposed model is shown in Figure 11b.

## CONCLUSIONS

Efficient metal sensitized photocyclization of the DTE in **1o** has been shown to occur via population of the $^3$IL state, as well as direct excitation of the $^1$IL state with UV light. These pathways have different energy barriers, as shown by the different temperature dependences of the photocyclization rates. Addition of a reductive quencher, DABCO, results in a slower rate of DTE photocyclization with irradiation with light at wavelengths greater than 420 nm, showing that this pathway involves an initially formed charge transfer site at the metal acetylide. With direct UV excitation the rate of photocyclization is unaffected by the addition of DABCO, supporting direct ring closing from the $^1$IL excited state in this case.

An important goal of this study was to examine the effect of the linker between the metal and the DTE on the photophysical behavior. A key result that has emerged is that the excited states involved in the metal sensitized photocyclization of **1o** (where the linker is a short, conjugated group) and **2o** (where the linker is longer and nonconjugated), are similar. The differences in photocyclization rate between the two complexes can be attributed to the poorer orbital overlap in **2o**. The photophysical behavior of the model complexes **4** and **5** provides interesting guidance for the design of complexes in which pendant DTE groups can be used to modulate the photophysical behavior of metal complexes. This is not possible in **1o** and **2o** because excitation of the metal results in energy transfer to the DTE and subsequent photocyclization. The excited state in complex **4** is a MLCT state, while addition of the thiophene in **5** results in population of either a $^3$CS or a $^3$IL state (or a combination of the two). The similarity in the TA spectra of **5** and **1o** or **2o** indicates that the presence of the phenylthiophene group is sufficient to cause the excited state to shift from the metal ($^3$MLCT) to ligand (phenylthiophene or DTE photoswitch). Either removing the phenyl group or breaking the conjugation between phenyl and thienyl groups could prevent energy transfer across the linker from metal to the uncyclized DTE. For this strategy to succeed, however, energy transfer to the photocyclized DTE would still have to occur to allow modulation of excited state chemistry at the metal.

## ASSOCIATED CONTENT

**Supporting Information.** Fitted time decay profiles of phosphorescence for **4** and **5**, and fitted time decay profiles of the TA signals for **1c**, **2o**, **2c**, **3**, **4**, and **5**. This material is available free of charge via the Internet at http://pubs.acs.org.

## AUTHOR INFORMATION

**Corresponding Author**

*E-mail: nbranda@sfu.ca (N.R.B.), mwolf@chem.ubc.ca (M.O.W.).

## ACKNOWLEDGMENT

This research was supported in part by the Natural Sciences and Engineering Research Council of Canada, the Canada Research Chairs Program, and Simon Fraser University. The assistance of Dr. Saeid Kamal (Laboratory for Advanced Spectroscopy and Imaging Research) is acknowledged.

## REFERENCES

(1) Kume, S.; Nishihara, H. *Dalton Trans.* **2008**, 3260–3271.
(2) Guerchais, V.; Le Bozec, H. *Top. Organomet. Chem.* **2010**, *28*, 171–225.
(3) Ko, C.-C.; Yam, V. W.-W. *J. Mater. Chem.* **2010**, *20*, 2063–2070.
(4) Fernandez-Acebes, A.; Lehn, J.-M. *Chem.—Eur. J.* **1999**, *5*, 3285–3292.
(5) Norsten, T. B.; Branda, N. R. *Adv. Mater.* **2001**, *13*, 347–349.
(6) Lee, I.; You, Y.; Lim, S.-J.; Park, S. Y. *Chem. Lett.* **2007**, *36*, 888–889.
(7) Green, K. A.; Cifuentes, M. P.; Corkery, T. C.; Samoc, M.; Humphrey, M. G. *Angew. Chem., Int. Ed.* **2009**, *48*, 7867–7870.
(8) Nakagawa, T.; Hasegawa, Y.; Kawai, T. *Chem. Commun.* **2009**, 5630–5632.
(9) Aubert, V.; Guerchais, V.; Ishow, E.; Hoang-Thi, K.; Ledoux, I.; Nakatani, K.; Le Bozec, H. *Angew. Chem., Int. Ed.* **2008**, *47*, 577–580.
(10) Tanaka, Y.; Inagaki, A.; Akita, M. *Chem. Commun.* **2007**, 1169–1171.

(11) Guirado, G.; Coudret, C.; Launay, J. P. *J. Phys. Chem. C* **2007**, *111*, 2770–2776.
(12) Lee, P. H. M.; Ko, C. C.; Zhu, N. Y.; Yam, V. W. W. *J. Am. Chem. Soc.* **2007**, *129*, 6058–6059.
(13) Motoyama, K.; Koike, T.; Akita, M. *Chem. Commun.* **2008**, 5812–5814.
(14) Liu, Y. F.; Lagrost, C.; Costuas, K.; Tchouar, N.; Le Bozec, H.; Rigaut, S. *Chem. Commun.* **2008**, 6117–6119.
(15) Castellano, F. N.; Pomestchenko, I. E.; Shikhova, E.; Hua, F.; Muro, M. L.; Rajapakse, N. *Coord. Chem. Rev.* **2006**, *250*, 1819–1828.
(16) Han, X.; Wu, L. Z.; Si, G.; Pan, J.; Yang, Q. Z.; Zhang, L. P.; Tung, C. H. *Chem.—Eur. J.* **2007**, *13*, 1231–1239.
(17) Michalec, J. F.; Bejune, S. A.; McMillin, D. R. *Inorg. Chem.* **2000**, *39*, 2708–2709.
(18) Yang, Q. Z.; Wu, L. Z.; Wu, Z. X.; Zhang, L. P.; Tung, C. H. *Inorg. Chem.* **2002**, *41*, 5653–5655.
(19) Guo, F. Q.; Sun, W. F.; Liu, Y.; Schanze, K. *Inorg. Chem.* **2005**, *44*, 4055–4065.
(20) Du, P. W.; Schneider, J.; Jarosz, P.; Eisenberg, R. *J. Am. Chem. Soc.* **2006**, *128*, 7726–7727.
(21) Du, P. W.; Schneider, J.; Jarosz, P.; Zhang, J.; Brennessel, W. W.; Eisenberg, R. *J. Phys. Chem. B* **2007**, *111*, 6887–6894.
(22) Feng, K.; Zhang, R. Y.; Wu, L. Z.; Tu, B.; Peng, M. L.; Zhang, L. P.; Zhao, D.; Tung, C. H. *J. Am. Chem. Soc.* **2006**, *128*, 14685–14690.
(23) Wang, X.; Goeb, S.; Ji, Z.; Pogulaichenko, N. A.; Castellano, F. N. *Inorg. Chem.* **2011**, *50*, 705–707.
(24) Yoon, T. P.; Ischay, M. A.; Du, J. N. *Nat. Chem.* **2010**, *2*, 527–532.
(25) Irie, M. *Chem. Rev.* **2000**, *100*, 1685–1716.
(26) Tian, H.; Wang, S. *Chem. Commun.* **2007**, 781–792.
(27) Lemieux, V.; Branda, N. R. *Org. Lett.* **2005**, *7*, 2969–2972.
(28) Samachetty, H. D.; Branda, N. R. *Chem. Commun.* **2005**, 2840–2842.
(29) Sud, D.; Norsten, T. B.; Branda, N. R. *Angew. Chem., Int. Ed.* **2005**, *44*, 2019–2021.
(30) Odo, Y.; Matsuda, K.; Irie, M. *Chem.—Eur. J.* **2006**, *12*, 4283–4288.
(31) Samachetty, H. D.; Branda, N. R. *Pure Appl. Chem.* **2006**, *78*, 2351–2359.
(32) Sud, D.; Wigglesworth, T. J.; Branda, N. R. *Angew. Chem., Int. Ed.* **2007**, *46*, 8017–8019.
(33) Lemieux, V.; Spantulescu, M. D.; Baldridge, K. K.; Branda, N. R. *Angew. Chem., Int. Ed.* **2008**, *47*, 5034–5037.
(34) Samachetty, H. D.; Lemieux, V.; Branda, N. R. *Tetrahedron* **2008**, *64*, 8292–8300.
(35) Vomasta, D.; Hogner, C.; Branda, N. R.; Konig, B. *Angew. Chem., Int. Ed.* **2008**, *47*, 7644–7647.
(36) Kozlov, D. V.; Castellano, F. N. *J. Phys. Chem. A* **2004**, *108*, 10619–10622.
(37) Roberts, M. N.; Nagle, J. K.; Finden, J. G.; Branda, N. R.; Wolf, M. O. *Inorg. Chem.* **2009**, *48*, 19–21.
(38) Yam, V. W.-W.; Ko, C.-C.; Zhu, N. *J. Am. Chem. Soc.* **2004**, *126*, 12734–12735.
(39) Ko, C.-C.; Kwok, W.-M.; Yam, V. W.-W.; Phillips, D. L. *Chem.—Eur. J.* **2006**, *12*, 5840–5848.
(40) Jukes, R. T. F.; Adamo, V.; Hartl, F.; Belser, P.; De Cola, L. *Inorg. Chem.* **2004**, *43*, 2779–2792.
(41) Indelli, M. T.; Carli, S.; Ghirotti, M.; Chiorboli, C.; Ravaglia, M.; Garavelli, M.; Scandola, F. *J. Am. Chem. Soc.* **2008**, *130*, 7286–7299.
(42) Lee, J. K.-W.; Ko, C.-C.; Wong, K. M.-C.; Zhu, N.; Yam, V. W.-W. *Organometallics* **2007**, *26*, 12–15.
(43) Finden, J.; Kunz, T. K.; Branda, N. R.; Wolf, M. O. *Adv. Mater.* **2008**, *20*, 1998–2002.
(44) Guerra, C. F.; Snijders, J. G.; te Velde, G.; Baerends, E. J. *Theor. Chem. Acc.* **1998**, *99*, 391–403.
(45) Velde, G. T.; Bickelhaupt, F. M.; Baerends, E. J.; Guerra, C. F.; Van Gisbergen, S. J. A.; Snijders, J. G.; Ziegler, T. *J. Comput. Chem.* **2001**, *22*, 931–967.
(46) van Lenthe, E.; Baerends, E. J.; Snijders, J. G. *J. Chem. Phys.* **1993**, *99*, 4597–4610.
(47) van Lenthe, E.; Baerends, E. J.; Snijders, J. G. *J. Chem. Phys.* **1994**, *101*, 9783–9792.
(48) van Lenthe, E.; Ehlers, A.; Baerends, E. J. *J. Chem. Phys.* **1999**, *110*, 8943–8953.
(49) Pye, C. C.; Ziegler, T. *Theor. Chem. Acc.* **1999**, *101*, 396–408.
(50) Rosa, A.; Baerends, E. J.; van Gisbergen, S. J. A.; van Lenthe, E.; Groeneveld, J. A.; Snijders, J. G. *J. Am. Chem. Soc.* **1999**, *121*, 10356–10365.
(51) van Gisbergen, S. J. A.; Snijders, J. G.; Baerends, E. J. *Comput. Phys. Commun.* **1999**, *118*, 119–138.
(52) Chakraborty, S.; Wadas, T. J.; Hester, H.; Flaschenreim, C.; Schmehl, R.; Eisenberg, R. *Inorg. Chem.* **2005**, *44*, 6284–6293.
(53) Shikhova, E.; Danilov, E. O.; Kinayyigit, S.; Pomestchenko, I. E.; Tregubov, A. D.; Camerel, F.; Retailleau, P.; Ziessel, R.; Castellano, F. N. *Inorg. Chem.* **2007**, *46*, 3038–3048.
(54) Tamai, N.; Miyasaka, H. *Chem. Rev.* **2000**, *100*, 1875–1890.
(55) Uchida, K.; Nakayama, Y.; Irie, M. *Bull. Chem. Soc. Jpn.* **1990**, *63*, 1311–1315.
(56) Irie, M.; Sakemura, K.; Okinaka, M.; Uchida, K. *J. Org. Chem.* **1995**, *60*, 8305–8309.
(57) Wang, X. Y.; Del Guerzo, A.; Schmehl, R. H. *J. Photochem. Photobiol., C* **2004**, *5*, 55–77.
(58) McGarrah, J. E.; Eisenberg, R. *Inorg. Chem.* **2003**, *42*, 4355–4365.
(59) Tyson, D. S.; Luman, C. R.; Zhou, X. L.; Castellano, F. N. *Inorg. Chem.* **2001**, *40*, 4063–4071.
(60) Hissler, M.; Harriman, A.; Khatyr, A.; Ziessel, R. *Chem.—Eur. J.* **1999**, *5*, 3366–3381.
(61) Ji, S. M.; Wu, W. H.; Wu, W. T.; Song, P.; Han, K. L.; Wang, Z. G.; Liu, S. S.; Guo, H. M.; Zhao, J. Z. *J. Mater. Chem.* **2010**, *20*, 1953–1963.
(62) Liu, X. J.; Feng, J. K.; Meng, J.; Pan, Q. J.; Ren, A. M.; Zhou, X.; Zhang, H. X. *Eur. J. Inorg. Chem.* **2005**, 1856–1866.